AIP | The Journal of Chemical Physics

Analytical energy gradient for the two-component normalized elimination of the small component method

Wenli Zou, Michael Filatov, and Dieter Cremer

Citation: The Journal of Chemical Physics **142**, 214106 (2015); doi: 10.1063/1.4921915
View online: http://dx.doi.org/10.1063/1.4921915
View Table of Contents: http://scitation.aip.org/content/aip/journal/jcp/142/21?ver=pdfcov
Published by the AIP Publishing

Analytical energy gradient for the two-component normalized elimination of the small component method

Wenli Zou, Michael Filatov, and Dieter Cremer[a)]
Computational and Theoretical Chemistry Group (CATCO), Department of Chemistry, Southern Methodist University, 3215 Daniel Ave, Dallas, Texas 75275-0314, USA

(Received 15 March 2015; accepted 20 May 2015; published online 4 June 2015)

The analytical gradient for the two-component Normalized Elimination of the Small Component (2c-NESC) method is presented. The 2c-NESC is a Dirac-exact method that employs the exact two-component one-electron Hamiltonian and thus leads to exact Dirac spin-orbit (SO) splittings for one-electron atoms. For many-electron atoms and molecules, the effect of the two-electron SO interaction is modeled by a screened nucleus potential using effective nuclear charges as proposed by Boettger [Phys. Rev. B **62**, 7809 (2000)]. The effect of spin-orbit coupling (SOC) on molecular geometries is analyzed utilizing the properties of the frontier orbitals and calculated SO couplings. It is shown that bond lengths can either be lengthened or shortened under the impact of SOC where in the first case the influence of low lying excited states with occupied antibonding orbitals plays a role and in the second case the jj-coupling between occupied antibonding and unoccupied bonding orbitals dominates. In general, the effect of SOC on bond lengths is relatively small ($\leq$5% of the scalar relativistic changes in the bond length). However, large effects are found for van der Waals complexes Hg_2 and Cn_2, which are due to the admixture of more bonding character to the highest occupied spinors. © *2015 AIP Publishing LLC.* [http://dx.doi.org/10.1063/1.4921915]

I. INTRODUCTION

In recent work, we have developed analytical first and second derivatives for the normalized elimination of the small component (NESC) method to calculate first and second order properties of relativistic atoms and molecules.[1–3] NESC was originally developed by Dyall[4] as a first principle 1- or 2-component (1c or 2c) approach, which is based on a decoupling of positive and negative energy states via the elimination of the small component of the relativistic wavefunction. In this respect, NESC is a *Dirac-exact* relativistic method: For one-electron atoms, it is fully equivalent to the 4-component (4c) Dirac equation.[5] Our previous method development work sets the basis for the routine scalar relativistic calculation of molecular geometries,[2] electric dipole moments,[3] EPR hyperfine structure constants,[6] contact densities for the calculation of Mössbauer isomer shifts,[7] or electric field gradients for nuclear quadrupole coupling constants.[8] As for the calculation of second order response properties, we developed the methodology for the analytic calculation of vibrational frequencies,[3,9] static electric polarizabilities, or infrared intensities[3] utilizing the 1c-NESC method. We applied these methods to predict molecular properties of mercury,[10] gold,[11] uranium containing molecules,[3] or other relativistic molecules.[12] In view of the importance of spin-orbit coupling (SOC) for atomic and molecular properties,[13–21] we extended, in another project, the 1c-NESC approach to a 2c-NESC method that reliably predicts the effects of SOC on the relative energies of relativistic systems.[22]

There are one- and two-electron contributions to the SOC operator where the latter reduce the former by about 5% in the case of elements with a filled 5d shell or about 10% in the case of elements with a filled 6d shell.[22,23] Although small, the two-electron terms cannot be neglected as they are important for obtaining reliable SOC corrections. Fortunately, the magnitude of the two-electron corrections varies parallel with the one-electron contributions (for exceptions, see Refs. 24 and 25) and therefore their calculation can be simplified thus significantly reducing the costs of 2c-NESC calculation.[22]

In previous work, we have used the screened-nuclear-spin-orbit (SNSO) approach of Boettger,[26] which is based on the observation that the two-electron contributions to SOC can be determined in an approximate form by appropriate screening of the nuclear potential, i.e., the use of effective nuclear charges. Originally, the SNSO approach was applied within the Douglas-Kroll-Hess (DKH) quasirelativistic approximation[27–29] and since it turned out to be a useful approximation of SOC effects, it was adopted by several authors in a similar way.[30–33] The spin-orbit (SO) splittings obtained with the SNSO approach reproduce the trends obtained with the exact Dirac-Fock-Coulomb values and deviate only by a few percentages from exact 4c-Dirac calculations.[22] By modification of the SNSO approach to mSNSO, a further improvement could be achieved[22] so that the 2c-NESC(mSNSO) method can easily compete with the atomic mean field integral (AMFI) approach[34] derived from the mean-field SOC operator of Hess and co-workers,[35] other 2c methods based on an effective one-electron SOC operator, or SOC calculations carried out with the Breit-Pauli operator.[36,37]

The 2c-NESC(mSNSO) method developed previously is based on the general Hartree-Fock (GHF) or general density functional theory (GDFT) formalism[38,39] for many-electron systems. To avoid confusion, we will speak of a 2c-NESC

a)Electronic address: dcremer@smu.edu.

method when one-electron systems have to be calculated and a 2c-NESC(mSNSO) method when many-electron systems are described. Other 2c-relativistic methods have been developed utilizing different starting points. Terms such as XQR (exact quasi-relativistic), IOTC (infinite order two-component),[40] or X2C (exact two-component) have been coined[41,42] where the latter term has replaced the former ones. The recent article by Peng and Reiher[19] critically reviews these terms. According to these authors, the term X2C (one-step exact decoupling transformation 2-component approach) should only be used provided certain requirements are fulfilled. Liu[43] pointed out that NESC is expressed in the *interaction picture (Dirac picture)* and becomes X2C when transformed to the *Schrödinger picture*. Unfortunately, some authors used X2C in connection with spin-free (sf) Dirac-exact methods, which leads to some confusion. To avoid any confusion, we continue to use the term Dirac-exact 2c-NESC to clarify that the basis of our work is the original NESC method by Dyall.[4]

Although the effect of SOC on molecular geometries has been investigated for either approximate all-electron methods such as the 2c-ZORA (zeroth order regular approximation)[44] or the 2c-ECP (effective core potential),[45,46] SOC investigations of molecular geometries have so far been done with numeric rather than analytical gradients.[47] Derivatives of the electric field gradient using 2c-relativistic methods[48,49] have been used and, at the 4c-DHF (Dirac-HF) and 4c-DKS (Dirac-Kohn-Sham) levels, analytical derivatives for geometry optimizations have been developed.[50–53] To the best of our knowledge, the current investigation presents for the first time an analytical 2c-NESC gradient, which can be routinely applied for the optimization of molecular geometries. We note in this connection that for this purpose, one has to start from the NESC Hamiltonian rather than simply using non-relativistic (NR) expressions for the analytic gradient because the latter can lead to picture change errors as was pointed out, e.g., by Kellö and Sadlej.[54]

The results of this work are presented in the following way. In Sec. II, we present the theory for calculating the 2c-NESC(SNSO)/GHF gradient. In this connection, we discuss also a significant improvement of the NESC-gradient previously published.[2] In Sec. III, computational details of our SOC gradient investigation are described, and in Sec. IV, the 2c-NESC(SNSO)/GDFT geometries of 32 molecules are analyzed. Section V summarizes the conclusions of the current SOC investigation.

II. ANALYTIC FIRST DERIVATIVE OF 2c-NESC

In the NESC method,[4] the four-component Dirac equation for one-electron system is transformed to a one- or two-component equation as given below,

$$\tilde{\mathbf{L}}\mathbf{A}_+ = \tilde{\mathbf{S}}\mathbf{A}_+\mathbf{E}_+, \tag{1}$$

which provides the exact electronic (positive energies, $\mathbf{E}_+$) solutions of the Dirac equation. The large-component relativistic electronic eigenvectors collected in matrix $\mathbf{A}_+$ are normalized utilizing the exact relativistic metric $\tilde{\mathbf{S}}$, where the NESC Hamiltonian $\tilde{\mathbf{L}}$ and the metric are given as

$$\tilde{\mathbf{L}} = \mathbf{U}^\dagger\mathbf{T} + \mathbf{T}\mathbf{U} - \mathbf{U}^\dagger(\mathbf{T} - \mathbf{W})\mathbf{U} + \mathbf{V}, \tag{2a}$$

$$\tilde{\mathbf{S}} = \mathbf{S} + \frac{1}{2mc^2}\mathbf{U}^\dagger\mathbf{T}\mathbf{U}. \tag{2b}$$

In Eq. (2), $\mathbf{S}$, $\mathbf{T}$, and $\mathbf{V}$ are the overlap, kinetic energy, and potential energy matrices; $\mathbf{U}$ is the matrix of the elimination of the small component operator, which connects the matrix of the eigenvectors of the large-component, $\mathbf{A}_+$, and matrix $\mathbf{B}_+$ of the pseudolarge-component eigenvectors via

$$\mathbf{B}_+ = \mathbf{U}\mathbf{A}_+. \tag{3}$$

$\mathbf{W}$ is the matrix of the operator $(\boldsymbol{\sigma}\cdot\mathbf{p})V(\mathbf{r})(\boldsymbol{\sigma}\cdot\mathbf{p})/4m^2c^2$, which can be split into the sf and SO part utilizing the Dirac identity $(\boldsymbol{\sigma}\cdot\mathbf{A})(\boldsymbol{\sigma}\cdot\mathbf{B}) = \mathbf{A}\cdot\mathbf{B} + i\boldsymbol{\sigma}\cdot\mathbf{A}\times\mathbf{B}$,

$$\mathbf{W} = \mathbf{W}_{sf} + i\boldsymbol{\sigma}\cdot\mathbf{W}_{so}. \tag{4}$$

Within the one-electron approximation to the many-body relativistic problem,[4,13,55] NESC Hamiltonian (2a) is renormalized on the non-relativistic metric

$$\mathbf{H}_{1e} = \mathbf{G}^\dagger\tilde{\mathbf{L}}\mathbf{G}, \tag{5}$$

where the renormalization matrix is given as[56]

$$\mathbf{G} = \mathbf{S}^{-1/2}\left(\mathbf{S}^{-1/2}\tilde{\mathbf{S}}\mathbf{S}^{-1/2}\right)^{-1/2}\mathbf{S}^{1/2} = \mathbf{S}^{-1/2}\mathbf{K}\,\mathbf{S}^{1/2} \tag{6}$$

and is employed in the context of the usual non-relativistic many-body formalism. If the SO part of $\mathbf{W}$ is retained as in the 2c-NESC method,[22] a two-component formalism is obtained based on either the GHF or GDFT methodology.[38,39] In the 2c case, all the matrices in the GHF total energy expression

$$E = tr\mathbf{P}\mathbf{H}_{2c} + \frac{1}{2}tr\mathbf{P}_{re}(\mathcal{J} - \mathcal{K}) \tag{7}$$

have doubled dimension as compared to their 1c-NESC and non-relativistic counterparts. In Eq. (7), $\mathbf{P} = \mathbf{C}\mathbf{n}\mathbf{C}^\dagger$ is the GHF density matrix ($\mathbf{C}$ are the GHF eigenvectors and $\mathbf{n}$ is a diagonal matrix of orbital occupation numbers). As only real basis functions are employed to compute the two-electron integrals, its real part $\boldsymbol{P}_{re} = Re(\boldsymbol{P})$ alone is sufficient to calculate the electron-electron repulsion energy. In the following, we will use the one-electron approximation exclusively and therefore the $1e$ subscript is dropped. Instead, the $2c$ prefix (or subscript) is used to emphasize the two-component nature of the NESC formalism.

Taking the derivative of the electronic energy with regard to λ, where λ can correspond to a nuclear coordinate, to a component of the electric field, etc., one obtains the analytic gradient of E,

$$\frac{\partial E}{\partial\lambda} = tr\boldsymbol{\Omega}_{re}\frac{\partial\mathbf{S}}{\partial\lambda} + tr\mathbf{P}\frac{\partial\mathbf{H}_{2c}}{\partial\lambda} + \frac{1}{2}tr\mathbf{P}_{re}\frac{\partial'}{\partial\lambda}(\mathcal{J} - \mathcal{K}). \tag{8}$$

Here, $\boldsymbol{\Omega}_{re} = Re(\boldsymbol{\Omega})$ where $\boldsymbol{\Omega}$ is defined by $\boldsymbol{\Omega} = -\mathbf{C}\boldsymbol{\epsilon}\mathbf{n}\mathbf{C}^\dagger$ and the prime at $\partial'/\partial\lambda$ implies that only the two-electron integrals rather than the density matrix need to be differentiated.

For the multiplications of doubled $\mathbf{P}$ and $\mathbf{X}$ matrices where $\mathbf{X}$ can be any real derivative matrices of $\mathbf{S}$, $\mathbf{T}$, $\mathbf{V}$, etc., the calculations can be simplified utilizing the relationship

$$\begin{aligned}\mathbf{P}_{2M\times2M}\mathbf{X}_{2M\times2M} &= \mathbf{P}^{\alpha\alpha}_{M\times M}\mathbf{X}^{\alpha\alpha}_{M\times M} + \mathbf{P}^{\beta\beta}_{M\times M}\mathbf{X}^{\beta\beta}_{M\times M}\\ &= \left(\mathbf{P}^{\alpha\alpha}_{M\times M} + \mathbf{P}^{\beta\beta}_{M\times M}\right)\mathbf{X}_{M\times M}\\ &= \left[Re\left(\mathbf{P}^{\alpha\alpha}_{M\times M}\right) + Re\left(\mathbf{P}^{\beta\beta}_{M\times M}\right)\right]\mathbf{X}_{M\times M},\end{aligned} \tag{9}$$

where $\mathbf{X}^{\alpha\alpha}_{M\times M} = \mathbf{X}^{\beta\beta}_{M\times M} = \mathbf{X}_{M\times M}$, $\mathbf{X}^{\alpha\beta}_{M\times M} = \mathbf{X}^{\beta\alpha}_{M\times M} = \mathbf{0}$, and M is the number of basis functions in the spin-free calculation. The first and the last terms on the rhs of Eq. (8) are calculated utilizing the non-relativistic GHF methodology. Only the second term has to be determined in a 2c-NESC gradient calculation.

According to Ref. 2, the derivative of the renormalized NESC Hamiltonian is

$$\frac{\partial \mathbf{H}_{2c}}{\partial\lambda} = \frac{\partial \mathbf{G}^\dagger}{\partial\lambda}\tilde{\mathbf{L}}\mathbf{G} + \mathbf{G}^\dagger\tilde{\mathbf{L}}\frac{\partial \mathbf{G}}{\partial\lambda} + \mathbf{G}^\dagger\frac{\partial\tilde{\mathbf{L}}}{\partial\lambda}\mathbf{G}, \tag{10}$$

and therefore the second term in Eq. (8) adopts the form

$$tr\mathbf{P}\frac{\partial \mathbf{H}_{2c}}{\partial\lambda} = tr\tilde{\mathbf{P}}\frac{\partial\tilde{\mathbf{L}}}{\partial\lambda} + tr\mathbf{D}\frac{\partial \mathbf{G}^\dagger}{\partial\lambda} + tr\mathbf{D}^\dagger\frac{\partial \mathbf{G}}{\partial\lambda}, \tag{11}$$

where the matrices $\tilde{\mathbf{P}} = \mathbf{G}\mathbf{P}\mathbf{G}^\dagger$ and $\mathbf{D} = \tilde{\mathbf{L}}\mathbf{G}\mathbf{P}$ are used.

The last two terms on the rhs of Eq. (11) can be calculated by Eq. (30) in Ref. 2. However, since $\mathbf{G}^2 = \tilde{\mathbf{S}}^{-1}\mathbf{S}$, calculations can be significantly simplified as will be shown in the following. In Ref. 9, it was proved that the renormalization matrix $\mathbf{G}$ used in the spin-free NESC method is positive definite ($p.d.$). This is also true for a complex matrix $\mathbf{G}$ of 2c-NESC. Because of Eq. (6), $\mathbf{G}$ and $\mathbf{K}$ are similar matrices. Hence, if one can prove that $\mathbf{K}$ is $p.d.$, $\mathbf{G}$ should also be $p.d$. Considering that $(\tilde{\mathbf{S}}^{-1/2})^\dagger = \tilde{\mathbf{S}}^{-1/2}$, one obtains

$$\mathbf{K}^2 = \mathbf{S}^{1/2}\tilde{\mathbf{S}}^{-1}\mathbf{S}^{1/2} = \left(\tilde{\mathbf{S}}^{-1/2}\mathbf{S}^{1/2}\right)^\dagger\left(\tilde{\mathbf{S}}^{-1/2}\mathbf{S}^{1/2}\right), \tag{12}$$

where it must be recalled that $\tilde{\mathbf{S}}$ is $p.d.$ (see Ref. 9). If $\mathbf{K}^2$ is multiplied by an arbitrary non-zero complex vector $\mathbf{x}$ on both sides and if $\mathbf{y} = \left(\tilde{\mathbf{S}}^{-1/2}\mathbf{S}^{1/2}\right)\mathbf{x}$, one can write

$$\mathbf{x}^\dagger\mathbf{K}^2\mathbf{x} = \mathbf{y}^\dagger\mathbf{y} = \sum_i |y_i|^2 \geq 0. \tag{13}$$

Since $\mathbf{x}$ is an arbitrary non-zero vector, Eq. (13) must lead to a positive value. Consequently, $\mathbf{K}^2$ is a $p.d.$ matrix. The square-roots of its eigenvalues are positive or negative real values. Usually only positive square-roots are taken into consideration, which implies that both matrices $\mathbf{K}$ and $\mathbf{G}$ are $p.d.$

Differentiating $\mathbf{G}^2$, one obtains

$$\frac{\partial(\mathbf{G}^2)}{\partial\lambda} = \frac{\partial \mathbf{G}}{\partial\lambda}\mathbf{G} + \mathbf{G}\frac{\partial \mathbf{G}}{\partial\lambda}. \tag{14}$$

Because of the similarity between matrix $\mathbf{G}$ and the Hermitian matrix $\mathbf{K}$, it follows that ($\mathbf{R}_K$ and $\mathbf{R}_G$ are respective eigenvectors)

$$\mathbf{K}\mathbf{R}_K = \mathbf{R}_K\mathbf{k}, \tag{15a}$$
$$\mathbf{G}\mathbf{R}_G = \mathbf{R}_G\mathbf{g}, \tag{15b}$$
$$\mathbf{R}_G = \mathbf{S}^{-1/2}\mathbf{R}_K, \tag{15c}$$
$$\mathbf{k} = \mathbf{g} = \mathbf{R}_G^{-1}\mathbf{G}\mathbf{R}_G, \tag{15d}$$

where the inverse of the non-hermitian eigenvector matrix $\mathbf{R}_G$ can be calculated according to $\mathbf{R}_G^{-1} = \mathbf{R}_K^\dagger\mathbf{S}^{1/2}$.

Although $\mathbf{G}$ is not Hermitian, $\mathbf{g}$ is real (because $\mathbf{G}$ is $p.d.$), which can be used to simplify the calculation. Eigenvector matrix $\mathbf{R}_G$ is real in the case of a spin-free NESC calculation, but complex for 2c-NESC. In view of the non-unitarity of $\mathbf{G}$, $\mathbf{R}_G^\dagger\mathbf{R}_G \neq \mathbf{I}$. Therefore, we have to modify the originally published procedure (Eqs. (25) and (27-29) of Ref. 2). By multiplying Eq. (14) with $\mathbf{R}_G^{-1}$ from the left and with $\mathbf{R}_G$ from the right and using Eqs. (15b) and (15d), one obtains

$$\begin{aligned}\mathbf{R}_G^{-1}\frac{\partial(\mathbf{G}^2)}{\partial\lambda}\mathbf{R}_G &= \mathbf{R}_G^{-1}\frac{\partial \mathbf{G}}{\partial\lambda}\mathbf{G}\mathbf{R}_G + \mathbf{R}_G^{-1}\mathbf{G}\frac{\partial \mathbf{G}}{\partial\lambda}\mathbf{R}_G \\ &= \mathbf{R}_G^{-1}\frac{\partial \mathbf{G}}{\partial\lambda}\mathbf{R}_G\mathbf{g} + \mathbf{g}\mathbf{R}_G^{-1}\frac{\partial \mathbf{G}}{\partial\lambda}\mathbf{R}_G,\end{aligned} \tag{16}$$

$$\left(\mathbf{R}_G^{-1}\frac{\partial \mathbf{G}}{\partial\lambda}\mathbf{R}_G\right)_{i,j} = \left(\mathbf{R}_G^{-1}\frac{\partial(\mathbf{G}^2)}{\partial\lambda}\mathbf{R}_G\right)_{i,j}\Big/(g_i + g_j). \tag{17}$$

By rearranging, it follows

$$\begin{aligned}\left(\frac{\partial \mathbf{G}}{\partial\lambda}\right)_{m,n} &= \sum_{i,j}(\mathbf{R}_G)_{m,i}(g_i + g_j)^{-1} \\ &\quad\times\left(\mathbf{R}_G^{-1}\frac{\partial(\mathbf{G}^2)}{\partial\lambda}\mathbf{R}_G\right)_{i,j}\left(\mathbf{R}_G^{-1}\right)_{j,n},\end{aligned} \tag{18}$$

which is equivalent to Eq. (27) of Ref. 2 for the scalar-relativistic NESC method apart from the fact that $\mathbf{C}^\dagger$ is replaced by $\mathbf{R}_G^{-1}$. By performing a similarity transformation as in Eq. (28) of Ref. 2, the following equations are obtained:

$$\begin{aligned}tr\mathbf{D}^\dagger\frac{\partial \mathbf{G}}{\partial\lambda} &= \sum_{m,n}\left(\mathbf{D}^\dagger\right)_{n,m}\left(\frac{\partial \mathbf{G}}{\partial\lambda}\right)_{m,n} \\ &= \sum_{i,j}\left(\mathbf{R}_G^{-1}\mathbf{D}^\dagger\mathbf{R}_G\right)_{j,i}(g_i + g_j)^{-1}\left(\mathbf{R}_G^{-1}\frac{\partial(\mathbf{G}^2)}{\partial\lambda}\mathbf{R}_G\right)_{i,j} \\ &= tr\mathbf{X}\mathbf{R}_G^{-1}\frac{\partial(\mathbf{G}^2)}{\partial\lambda}\mathbf{R}_G = tr\mathbf{Z}\frac{\partial(\mathbf{G}^2)}{\partial\lambda},\end{aligned} \tag{19}$$

where two new matrices are introduced: $\mathbf{X}$ with the elements $X_{j,i} = \left(\mathbf{R}_G^{-1}\mathbf{D}^\dagger\mathbf{R}_G\right)_{j,i}/\left(g_i + g_j\right)$ and $\mathbf{Z} = \mathbf{R}_G\mathbf{X}\mathbf{R}_G^{-1}$. Since $\mathbf{G}$ is $p.d.$, the denominator $g_i + g_j$ is non-zero. Utilizing Eq. (19) and $\mathbf{G}^2 = \tilde{\mathbf{S}}^{-1}\mathbf{S}$, the last two terms on the rhs of Eq. (11) become

$$\begin{aligned}&tr\mathbf{D}\frac{\partial \mathbf{G}^\dagger}{\partial\lambda} + tr\mathbf{D}^\dagger\frac{\partial \mathbf{G}}{\partial\lambda} \\ &= tr\left[\mathbf{Z}^\dagger\frac{\partial(\mathbf{G}^2)}{\partial\lambda}^\dagger + \mathbf{Z}\frac{\partial(\mathbf{G}^2)}{\partial\lambda}\right] \\ &= tr\left(\mathbf{Z}\tilde{\mathbf{S}}^{-1} + \tilde{\mathbf{S}}^{-1}\mathbf{Z}^\dagger - \mathbf{Y}\right)\frac{\partial \mathbf{S}}{\partial\lambda} - \frac{1}{2mc^2}tr\mathbf{U}\mathbf{Y}\mathbf{U}^\dagger\frac{\partial \mathbf{T}}{\partial\lambda} \\ &\quad - \frac{1}{2mc^2}tr\left(\mathbf{T}\mathbf{U}\mathbf{Y}\frac{\partial \mathbf{U}^\dagger}{\partial\lambda} + \mathbf{Y}\mathbf{U}^\dagger\mathbf{T}\frac{\partial \mathbf{U}}{\partial\lambda}\right) \\ &= tr\mathbf{P}_{GS}\frac{\partial \mathbf{S}}{\partial\lambda} + tr\mathbf{P}_{GT}\frac{\partial \mathbf{T}}{\partial\lambda} + tr\left(\mathbf{P}_{GU}^\dagger\frac{\partial \mathbf{U}^\dagger}{\partial\lambda} + \mathbf{P}_{GU}\frac{\partial \mathbf{U}}{\partial\lambda}\right),\end{aligned} \tag{20}$$

where $\mathbf{Y} = \tilde{\mathbf{S}}^{-1}\left(\mathbf{S}\mathbf{Z} + \mathbf{Z}^\dagger\mathbf{S}\right)\tilde{\mathbf{S}}^{-1}$.

For comparison, the method introduced in Ref. 2 has to carry out three transformations (from $\mathbf{D}_i$ to $\mathbf{D}_{iz}$ with $i = 0$, 1, and 2), whereas the new method described above requires only one transformation, which makes it faster and more accurate.

The derivatives of the matrix $\tilde{\mathbf{L}}$ are

$$\begin{aligned}\frac{\partial\tilde{\mathbf{L}}}{\partial\lambda} &= \mathbf{U}^\dagger\frac{\partial \mathbf{T}}{\partial\lambda} + \frac{\partial \mathbf{T}}{\partial\lambda}\mathbf{U} - \mathbf{U}^\dagger\frac{\partial \mathbf{T}}{\partial\lambda}\mathbf{U} + \mathbf{U}^\dagger\frac{\partial \mathbf{W}}{\partial\lambda}\mathbf{U} + \frac{\partial \mathbf{V}}{\partial\lambda} \\ &\quad + \frac{\partial \mathbf{U}^\dagger}{\partial\lambda}\left[\mathbf{T} - (\mathbf{T} - \mathbf{W})\,\mathbf{U}\right] \\ &\quad + \left[\mathbf{T} - \mathbf{U}^\dagger(\mathbf{T} - \mathbf{W})\right]\frac{\partial \mathbf{U}}{\partial\lambda},\end{aligned} \tag{21}$$

where $\frac{\partial \mathbf{U}}{\partial \lambda}$ can be calculated with the help of response theory and expressed entirely in terms of the derivatives of **S**, **T**, **V**, **W** and the corresponding transformed density matrices $\mathbf{P}_{US}$, $\mathbf{P}_{UT}$, $\mathbf{P}_{UV}$, and $\mathbf{P}_{UW}$ (see Appendix B in Ref. 9).

Then, Eq. (11) can be calculated according to

$$tr\mathbf{P}\frac{\partial \mathbf{H}_{2c}}{\partial \lambda} = tr\mathbf{P}_{GS}\frac{\partial \mathbf{S}}{\partial \lambda} + tr\left(\mathbf{U}\tilde{\mathbf{P}} + \tilde{\mathbf{P}}\mathbf{U}^{\dagger} - \mathbf{U}\tilde{\mathbf{P}}\mathbf{U}^{\dagger} + \mathbf{P}_{GT}\right)\frac{\partial \mathbf{T}}{\partial \lambda} + tr\tilde{\mathbf{P}}\frac{\partial \mathbf{V}}{\partial \lambda} + tr\left(\mathbf{U}\tilde{\mathbf{P}}\mathbf{U}^{\dagger}\right)\frac{\partial \mathbf{W}}{\partial \lambda} + tr\left(\mathbf{P}_U^{\dagger}\frac{\partial \mathbf{U}^{\dagger}}{\partial \lambda} + \mathbf{P}_U\frac{\partial \mathbf{U}}{\partial \lambda}\right) \tag{22}$$

$$\begin{aligned} &= tr\left(\mathbf{P}_{GS} + \mathbf{P}_{US} + \mathbf{P}_{US}^{\dagger}\right)\frac{\partial \mathbf{S}}{\partial \lambda} + tr\left(\mathbf{U}\tilde{\mathbf{P}} + \tilde{\mathbf{P}}\mathbf{U}^{\dagger} - \mathbf{U}\tilde{\mathbf{P}}\mathbf{U}^{\dagger} + \mathbf{P}_{GT} + \mathbf{P}_{UT} + \mathbf{P}_{UT}^{\dagger}\right)\frac{\partial \mathbf{T}}{\partial \lambda} + tr\left(\tilde{\mathbf{P}} + \mathbf{P}_{UV} + \mathbf{P}_{UV}^{\dagger}\right)\frac{\partial \mathbf{V}}{\partial \lambda} \\ &+ tr\left(\mathbf{U}\tilde{\mathbf{P}}\mathbf{U}^{\dagger} + \mathbf{P}_{UW} + \mathbf{P}_{UW}^{\dagger}\right)\frac{\partial \mathbf{W}}{\partial \lambda} = tr\mathbf{P}_S\frac{\partial \mathbf{S}}{\partial \lambda} + tr\mathbf{P}_T\frac{\partial \mathbf{T}}{\partial \lambda} + tr\mathbf{P}_V\frac{\partial \mathbf{V}}{\partial \lambda} + tr\mathbf{P}_W\frac{\partial \mathbf{W}}{\partial \lambda}, \end{aligned} \tag{23}$$

where

$$\mathbf{P}_U = \tilde{\mathbf{P}}\left[\mathbf{T} - \mathbf{U}^{\dagger}(\mathbf{T} - \mathbf{W})\right] + \mathbf{P}_{GU}. \tag{24}$$

Usually the contributions from the first and second terms on the rhs of Eq. (24) are in the same order of magnitude but may have opposite signs so that they make a small but significant contribution to the gradient in the case of steep basis functions. Since all NESC calculations are carried out on the basis of a *first-diagonalize-then-contract* strategy,[1] they both have to be calculated. In the NESC program,[57] the last term of Eq. (22) is calculated by default unless the exponent of the steepest basis function is smaller than 1×10^6 (i.e., $\mathbf{P}_U = \mathbf{0}$ because of its contributions to the gradient being smaller than 10^{-9}).

Since the derivatives of **S**, **T**, and **V** are real, one can take the real $\alpha\alpha$ and $\beta\beta$ parts of the **P**-dependent matrices (see Eq. (9)), which implies that the non-relativistic derivative subroutines can be used. Only the last term in Eq. (23) has to be programmed, which can be obtained according to

$$\begin{aligned} tr\mathbf{P}_W\frac{\partial \mathbf{W}}{\partial \lambda} &= tr\mathbf{P}_W^{\alpha\alpha}\frac{\partial \mathbf{W}^{\alpha\alpha}}{\partial \lambda} + tr\mathbf{P}_W^{\alpha\beta}\frac{\partial \mathbf{W}^{\beta\alpha}}{\partial \lambda} + tr\mathbf{P}_W^{\beta\alpha}\frac{\partial \mathbf{W}^{\alpha\beta}}{\partial \lambda} + tr\mathbf{P}_W^{\beta\beta}\frac{\partial \mathbf{W}^{\beta\beta}}{\partial \lambda} \\ &= tr\left(\mathbf{P}_W^{\alpha\alpha} + \mathbf{P}_W^{\beta\beta}\right)\frac{\partial \mathbf{W}_{sf}}{\partial \lambda} - i\,tr\left(\mathbf{P}_W^{\alpha\alpha} - \mathbf{P}_W^{\beta\beta}\right)\frac{\partial \mathbf{W}_z}{\partial \lambda} - i\,tr\left(\mathbf{P}_W^{\alpha\beta} + \mathbf{P}_W^{\beta\alpha}\right)\frac{\partial \mathbf{W}_x}{\partial \lambda} + tr\left(\mathbf{P}_W^{\alpha\beta} - \mathbf{P}_W^{\beta\alpha}\right)\frac{\partial \mathbf{W}_y}{\partial \lambda} \\ &= tr\,Re\left(\mathbf{P}_W^{\alpha\alpha} + \mathbf{P}_W^{\beta\beta}\right)\frac{\partial \mathbf{W}_{sf}}{\partial \lambda} + tr\,Im\left(\mathbf{P}_W^{\alpha\alpha} - \mathbf{P}_W^{\beta\beta}\right)\frac{\partial \mathbf{W}_z}{\partial \lambda} + tr\,Im\left(\mathbf{P}_W^{\alpha\beta} + \mathbf{P}_W^{\beta\alpha}\right)\frac{\partial \mathbf{W}_x}{\partial \lambda} + tr\,Re\left(\mathbf{P}_W^{\alpha\beta} - \mathbf{P}_W^{\beta\alpha}\right)\frac{\partial \mathbf{W}_y}{\partial \lambda}. \end{aligned} \tag{25}$$

To distinguish between the symbols used in the general case as, for example, in Eq. (4), here the matrix **W** is rewritten in the form $\mathbf{W} = \mathbf{W}_{sf}^{(2)} - i\boldsymbol{\sigma}\cdot\mathbf{W}_{so}$. The $\mathbf{W}_{so}$ term is defined by $1/(4m^2c^2)\boldsymbol{\nabla}\times(-V)\boldsymbol{\nabla}$ since the V operator contains a negative sign. $\mathbf{W}_{sf}^{(2)}$ is given by a $2M \times 2M$ matrix in which each element of $\mathbf{W}_{sf}$ is expanded to a 2×2 block: The diagonal elements of the block keep the values of $\mathbf{W}_{sf}$ whereas the two off-diagonal elements are zero. Hence, the matrix elements of **W** are given by

$$\begin{pmatrix} W^{\alpha\alpha}(2\mu-1,2\nu-1) & W^{\alpha\beta}(2\mu-1,2\nu) \\ W^{\beta\alpha}(2\mu,2\nu-1) & W^{\beta\beta}(2\mu,2\nu) \end{pmatrix} = \begin{pmatrix} W_{sf}(\mu,\nu) - iW_z(\mu,\nu) & -iW_x(\mu,\nu) - W_y(\mu,\nu) \\ -iW_x(\mu,\nu) + W_y(\mu,\nu) & W_{sf}(\mu,\nu) + iW_z(\mu,\nu) \end{pmatrix}, \tag{26}$$

where indices μ and ν refer to basis functions. If the SNSO method is applied to $\mathbf{W}_{so}$ according to

$$\begin{aligned} \mathbf{W}_{SNSO} &= \mathbf{W}_{sf}^{(2)} - i\boldsymbol{\sigma}\cdot(\mathbf{W}_{so} - \mathbf{Q}\mathbf{W}_{so}\mathbf{Q}) \\ &= \mathbf{W} - \mathbf{Q}\left(\mathbf{W} - \mathbf{W}_{sf}^{(2)}\right)\mathbf{Q}, \end{aligned} \tag{27}$$

where **Q** is a diagonal matrix with diagonal elements being equal to the square root of the SNSO factors,[22] then the last term in Eq. (23) should be replaced by

$$\begin{aligned} tr\mathbf{P}_W\frac{\partial \mathbf{W}_{SNSO}}{\partial \lambda} &= tr\mathbf{P}_W\frac{\partial \mathbf{W}}{\partial \lambda} - tr\mathbf{Q}\mathbf{P}_W\mathbf{Q}\left(\frac{\partial \mathbf{W}}{\partial \lambda} - \frac{\partial \mathbf{W}_{sf}^{(2)}}{\partial \lambda}\right) \\ &= tr\left(\mathbf{P}_W - \mathbf{Q}\mathbf{P}_W\mathbf{Q}\right)\frac{\partial \mathbf{W}}{\partial \lambda} \\ &+ tr\mathbf{Q}\mathbf{P}_W\mathbf{Q}\frac{\partial \mathbf{W}_{sf}^{(2)}}{\partial \lambda}. \end{aligned} \tag{28}$$

If $\mathbf{P}_{so} = \mathbf{P}_W - \mathbf{Q}\mathbf{P}_W\mathbf{Q}$, Eq. (28) can be developed in a similar way as Eq. (25),

$$\begin{aligned} tr\mathbf{P}_W\frac{\partial \mathbf{W}_{SNSO}}{\partial \lambda} &= tr\,Re\left(\mathbf{P}_W^{\alpha\alpha} + \mathbf{P}_W^{\beta\beta}\right)\frac{\partial \mathbf{W}_{sf}}{\partial \lambda} \\ &+ tr\,Im\left(\mathbf{P}_{so}^{\alpha\alpha} - \mathbf{P}_{so}^{\beta\beta}\right)\frac{\partial \mathbf{W}_z}{\partial \lambda} \\ &+ tr\,Im\left(\mathbf{P}_{so}^{\alpha\beta} + \mathbf{P}_{so}^{\beta\alpha}\right)\frac{\partial \mathbf{W}_x}{\partial \lambda} \\ &+ tr\,Re\left(\mathbf{P}_{so}^{\alpha\beta} - \mathbf{P}_{so}^{\beta\alpha}\right)\frac{\partial \mathbf{W}_y}{\partial \lambda}. \end{aligned} \tag{29}$$

III. COMPUTATIONAL DETAILS

The algorithm described above has been implemented within the program package COLOGNE2015.[57] This implied the programming of the 2c-NESC gradient and the derivatives of the **W**-integrals, as well as the implementation of the gradient into a general purpose 2c-NESC program. All calculations are based on a finite nucleus model possessing a Gaussian

charge distribution.[13,58] A value of 137.035 999 070(98) a.u. was used for the velocity of light c.[59]

When calculating the analytical gradient of 2c-NESC and utilizing for the two-electron part the SNSO approach,[26] the matrix $\mathbf{W}_{so}$ is first scaled by suitable screening factors $\sqrt{Q(l_\mu)/Z_\mu}$ on both sides and then the Dirac equation is solved and the NESC matrix $\mathbf{H}_{2c-NESC}$ is formed. Such a procedure was also applied by van Wüllen and Michauk in connection with the 2c-DKH SOC method to speed up higher order 2c-DKH calculations.[32] In Table I, the effect of different scaling procedures on the accuracy of SOC splittings in the case of the noble gas element Uuo (E118) is demonstrated. Calculations were carried out with an uncontracted $32s30p20d15f$ basis where the exponents were generated by the formula[60,61]

$$\exp(-3.84 + 0.72 \times (i-1)), i = 1,2,\ldots,N_l, \qquad (30)$$

with $N_l = 32$ for s-, 30 for p-, 20 for d-, and 15 for f-type functions. For the 4c-DHF reference calculations, the relativistic program DIRAC was used.[53] All 2c-NESC SOC calculations[22] were performed with the GHF method and the program package COLONGE2015.[57] The following abbreviations are used: (i) 1eSO: only the one-electron part of the SOC Hamiltonian is calculated; (ii) SNSO(H): SNSO is used for the two-electron SO part of 2c-NESC Hamiltonian matrix $\mathbf{H}_{so}$; (iii) SNSO(W): SNSO is used for matrix $\mathbf{W}_{so}$; (iv) mSNSO(H) and mSNSO(W): a modified SNSO procedure is used[22] in (ii) and (iii), respectively.

The exact SOC splittings of the 4c-DHF method are best reproduced by the mSNSO procedure as is reflected by the maximum and the averaged errors given in percentage where mSNSO(H) scaling is only slightly better than the mSNSO(W) scaling. In other words, the loss of accuracy when scaling matrix $\mathbf{W}_{so}$ rather than matrix $\mathbf{H}_{so}$ is insignificant and therefore mSNSO(W) can be used for the 2c-NESC gradient calculations. The original SNSO scaling is less accurate but nevertheless reveals the necessity of including the two-electron part of SOC. The 1eSO values strongly differ from the exact 4c-DHF SOC splittings (Table I).

In Table II, the basis sets employed for the 2c-NESC geometry optimization of 32 different molecules are summarized. For reasons of comparison, the geometry optimizations have also been carried out with the 1c-NESC (= NESC) method using the same basis sets. For all calculations, GDFT with the PBE0 hybrid functional[62,63] was used. NR reference calculations were carried out with the same XC functional where for light atoms, the original def2-QZVPP basis sets[64] were employed. For heavy atoms, the relativistic basis sets of Table II were converted into non-relativistic basis sets by taking the contraction coefficients from HF atom calculations.

The accuracy of the analytical 2c-NESC gradient program was tested by comparison with optimized geometries based on a numerically determined gradient. Deviations in calculated bond lengths are 1×10^{-4} Å or smaller with a tendency of the numerical bond lengths being slightly longer. A deviation of 4×10^{-4} Å was obtained for the copernicium (eka-mercury) dimer, Cn_2, for which the numerical gradient is only accurate by 1×10^{-3} Å and the SOC has a strong impact on the bond length (see values in Table III).

IV. RESULTS AND DISCUSSION

Optimized NESC and 2c-NESC geometries of 32 molecules are listed in Table III. In Figure 1, changes in the bond lengths ΔR_{sr} and ΔR_{soc} due to scalar relativistic and SOC effects, respectively, are presented in form of two bar diagrams where the upper bar diagram gives the signed changes and the lower bar diagram gives, for simplifying the comparison, the absolute ΔR values.

In general, SOC effects on calculated bond lengths are relatively small compared to scalar relativistic effects (for a

TABLE I. SO splittings (in hartree) and errors (in %) of Uuo using 4c-DHF and 2c-NESC/GHF with different screening methods.

Splitting	4c-DHF	1eSO	SNSO(H)	mSNSO(H)	SNSO(W)	mSNSO(W)
2p	543.158	554.278	539.401	540.405	541.587	542.006
3p	133.390	136.129	132.615	133.009	133.100	133.307
4p	38.997	39.824	38.810	38.935	38.948	39.015
5p	11.522	11.779	11.474	11.511	11.515	11.535
6p	2.861	2.926	2.849	2.859	2.859	2.865
7p	0.434	0.444	0.432	0.434	0.433	0.435
3d	20.969	23.248	21.304	21.099	21.329	21.127
4d	5.914	6.609	6.037	5.979	6.044	5.987
5d	1.592	1.788	1.630	1.615	1.632	1.617
6d	0.271	0.306	0.279	0.276	0.279	0.277
4f	1.740	2.333	1.777	1.761	1.778	1.761
5f	0.368	0.501	0.382	0.378	0.382	0.378
Max $\Delta\epsilon$[a]		36.1	3.8	2.7	3.8	2.7
Av. $\Delta\epsilon(p)$		2.2	0.5	0.2	0.2	0.1
Av. $\Delta\epsilon(d)$		12.0	2.3	1.3	2.3	1.4
Av. $\Delta\epsilon(f)$		35.1	3.0	2.0	3.0	2.0
Av. $\Delta\epsilon$		10.9	1.5	0.8	1.4	0.9

[a]The maximum (Max) error in calculated spinor energies $\Delta\epsilon$ and the average (Av.) errors are given, where in the latter case, the corresponding errors for p, d, and f spinors are given separately.

TABLE II. Specification of the basis sets used in this work.

Element	Description	References
H, C, O, F, Cl, Br	NESC-recontracted def2-QZVPP	64
I, Os, Au, Hg, At, Th, U	NESC-recontracted SARC	71 and 72
U in CUO	DK3-Gen-Tk/NOSeC-VTZP	73 and 74
Hs (E108)	Dyall's triple-ζ basis set (32s29p20d13f), augmented by 1f2g, and recontracted to [19s15p12d9f2g] by NESC	75
Cn (E112)	Dyall's triple-ζ basis set (32s29p20d13f), uncontracted	75

general discussion of SOC effects on molecular properties, see Chap. 22 of Ref. 13). Scalar relativistic effects lead to a shortening of the bond length when *s*- and/or *p*-orbitals dominate bonding,[2] whereas a strong influence of *d*- or *f*-orbitals leads to a bond lengthening as was, e.g., shown by de Jong and co-workers in the case of the uranyl-dication[65] and what becomes also apparent for the CU and UO bonds of CUO (see Table III and Figure 1). This is in line with the scalar relativistic contraction or expansion of orbitals.[13] The scalar relativistic ΔR_{sr} values listed in Table III help to compare and analyze SOC related changes in the bond lengths. SOC can also lead to either a lengthening of the bond as found, for example, for the HX molecules or to a shortening of the bond length (most HgX_2 molecules).

SOC caused changes in the bond lengths are small ($<10^{-2}$ Å) for most closed shell molecules containing relativistic atoms (see Figure 1). Larger changes are obtained (10%-25% of the scalar relativistic changes) if the system in question

TABLE III. PBE0 optimized bond lengths (in Å) as obtained by NR, spin-free NESC, and 2c-NESC(mSNSO) calculations. The $L-S$ state or spin-orbit state is given before the slash whereas after the slash, the Ω state or general spinor state is given.

No.	Molecule	Symmetry	State	Bond	NR	NESC	2c-NESC	ΔR_{sr}	ΔR_{soc}	Expt.
1	HF	$C_{\infty v}$	$^1\Sigma^+ / 0^+$	H–F	0.9176	0.9178	0.9178	0.0002	0.0000	0.917[69]
2	HCl	$C_{\infty v}$	$^1\Sigma^+ /0^+$	H–Cl	1.2778	1.2778	1.2778	0.0000	0.0000	1.275[69]
3	HBr	$C_{\infty v}$	$^1\Sigma^+ / 0^+$	H–Br	1.4198	1.4180	1.4184	−0.0018	0.0004	1.414[69]
4	HI	$C_{\infty v}$	$^1\Sigma^+ / 0^+$	H–I	1.6154	1.6090	1.6109	−0.0064	0.0019	1.609[69]
5	HAt	$C_{\infty v}$	$^1\Sigma^+ / 0^+$	H–At	1.7195	1.6969	1.7279	−0.0226	0.0310	
6	AuH	$C_{\infty v}$	$^1\Sigma^+ / 0^+$	Au–H	1.7327	1.5302	1.5297[a]	−0.2025	−0.0005	1.524[69]
7	AuF	$C_{\infty v}$	$^1\Sigma^+ / 0^+$	Au–F	2.1034	1.9234	1.9161[a]	−0.1800	−0.0073	1.918[76]
8	AuCl	$C_{\infty v}$	$^1\Sigma^+ / 0^+$	Au–Cl	2.4229	2.2086	2.2040	−0.2143	−0.0046	2.199[77]
9	AuBr	$C_{\infty v}$	$^1\Sigma^+ / 0^+$	Au–Br	2.5348	2.3319	2.3299	−0.2029	−0.0020	2.318[77]
10	Au_2	$D_{\infty h}$	$^1\Sigma_g^+ / 0_g^+$	Au–Au	2.7664	2.5061	2.5014	−0.2603	−0.0047	2.472[78]
11	HgH	$C_{\infty v}$	$^2\Sigma^+ / 1/2$	Hg–H	1.8557	1.7468	1.7309	−0.1089	−0.0159	1.741[79]
12	HgH_2	$D_{\infty h}$	$^1\Sigma_g^+ / 0_g^+$	Hg–H	1.7694	1.6394	1.6352	−0.1300	−0.0042	1.633[80]
13	HgH_4	D_{4h}	$^1A_{1g} / A_{1g}$	Hg–H	1.7274	1.6247	1.6228	−0.1027	−0.0019	
14	HgF	$C_{\infty v}$	$^2\Sigma^+ / 1/2$	Hg–F	2.0939	2.0394	2.0341	−0.0545	−0.0053	
15	HgF_2	$D_{\infty h}$	$^1\Sigma_g^+ / 0_g^+$	Hg–F	2.0261	1.9104	1.9085	−0.1157	−0.0019	
16	HgF_4	D_{4h}	$^1A_{1g} / A_{1g}$	Hg–F	1.9628	1.8826	1.8823	−0.0802	−0.0003	
17	HgCl	$C_{\infty v}$	$^2\Sigma^+ / 1/2$	Hg–Cl	2.4647	2.3894	2.3820[a]	−0.0753	−0.0074	2.395[81]
18	$HgCl_2$	$D_{\infty h}$	$^1\Sigma_g^+ / 0_g^+$	Hg–Cl	2.3751	2.2492	2.2468	−0.1259	−0.0024	
19	$HgCl_4$	D_{4h}	$^1A_{1g} / A_{1g}$	Hg–Cl	2.3993	2.2949	2.2934	−0.1044	−0.0015	
20	HgBr	$C_{\infty v}$	$^2\Sigma^+ / 1/2$	Hg–Br	2.5947	2.5338	2.5289	−0.0609	−0.0049	2.62[82]
21	$HgBr_2$	$D_{\infty h}$	$^1\Sigma_g^+ / 0_g^+$	Hg–Br	2.5041	2.3849	2.3829	−0.1192	−0.0020	
22	$HgBr_4$	D_{4h}	$^1A_{1g} / A_{1g}$	Hg–Br	2.5600	2.4549	2.4561	−0.1051	0.0012	
23	HgI	$C_{\infty v}$	$^2\Sigma^+ / 1/2$	Hg–I	2.7931	2.7362	2.7511	−0.0569	0.0149	2.81[83]
24	HgI_2	$D_{\infty h}$	$^1\Sigma_g^+ / 0_g^+$	Hg–I	2.6932	2.5709	2.5726	−0.1223	0.0017	
25	HgI_4	D_{4h}	$^1A_{1g} / A_{1g}$	Hg–I	2.7935	2.6785	2.6941	−0.1150	0.0156	
26	Hg_2	$D_{\infty h}$	$^1\Sigma_g^+ / 0_g^+$	Hg–Hg	3.5866	3.5868	3.5392	0.0002	−0.0476	3.629[84]
27	ThO	$C_{\infty v}$	$^1\Sigma^+ / 0^+$	Th–O	1.8198	1.8258	1.8247	0.0060	−0.0011	1.840[85]
28	CUO	$C_{\infty v}$	$^1\Sigma^+ / 0^+$	U–C	1.7064	1.7345	1.7247	0.0281	−0.0098	
				U–O	1.7335	1.7787	1.7587	0.0452	−0.0200	
29	UF_6	O_h	$^1A_{1g} / A_{1g}$	U–F	2.0085	1.9938	1.9900	−0.0147	−0.0038	1.996[86]
30	OsO_4	T_d	$^1A_1 / A_1$	Os–O	1.7215	1.6856	1.6858	−0.0359	0.0002	1.684[87]
31	HsO_4	T_d	$^1A_1 / A_1$	Hs–O	1.8217	1.7570	1.7610[a]	−0.0647	0.0040	
32	Cn_2	$D_{\infty h}$	$^1\Sigma_g^+ / 0_g^+$	Cn–Cn	3.9015	3.6999	3.2546[a,b]	−0.2016	−0.4453	

[a]Also optimized numerically. AuH: 1.5297, AuF: 1.9161, HgCl: 2.3820, HsO_4: 1.7611, and Cn_2: 3.255.

[b]Other results in this work using the same functional and basis functions. 2-NESC(mSNSO(H)): 3.258 (*num.*), 2c-NESC(SO) 3.2064 (*ana.*), 2c-X2C/AMFI: 3.261 (*num.*), and 4c-DKS(LL + LS + SS + Gaunt): 3.256 (*num.*).

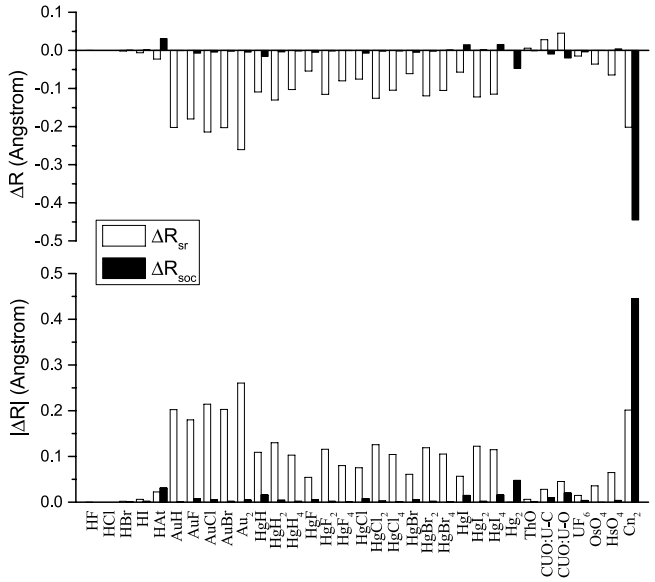

FIG. 1. Graphical representation of scalar relativistic and spin-orbit coupling changes ΔR_{sr} and ΔR_{soc} of the calculated bond lengths. Top: signed values and bottom: absolute values.

is characterized by a fractional occupation of p-, d-, or f-orbitals as in the case of the $HgX(^2\Sigma^+)$ radicals. In general, SOC effects on the bond length increase with increasing atomic number as can be seen for the HX series. Unusually, large SOC effects (both absolute values and relative ones in comparison with the scalar relativistic changes) are found for the van der Waals complexes Hg_2 and Cn_2.

The SOC effects on the bond lengths are too small to be decisive for getting a better agreement with the experimentally based r_e-geometries (apart from a small improvement in the case of the AuX molecules, see Table III and Figure 1). For the purpose of getting accurate r_e-values, coupled cluster (CC) theory with larger basis sets in connection with the 2c-NESC methodology would be needed. In this work, we are interested in analyzing the overall impact of SOC on scalar relativistic geometries and try to identify general trends in 2c-NESC geometries for which the PBE0 functional is sufficient. In the following, we will discuss SOC effects on the bond lengths by considering groups of molecules. In each case, we will identify the scalar relativistic frontier orbitals (HOMO and LUMO) and then consider how SOC leads to a mixing between these orbitals and how this can affect the bond length. For this purpose, graphical representations of frontier orbitals of a number of reference molecules are shown in Figure 2. In some cases, we will explicitly discuss bonding features of the frontier spinors, HOMS (highest occupied molecular spinor), HOMS−1, LUMS (lowest unoccupied molecular spinor), LUMS+1, etc.

H–X molecules. With increasing atomic number of X, the H–X bond length increases by $\Delta R_{soc} = 4$ (Br), 19 (I), and 310×10^{-4} Å (At, see Table III). This increase is related to an increased SO-splitting of the ^2P state for heavier X atoms: The valence p(X)-orbitals split into low-lying $p_{1/2}$ and high-lying $p_{3/2}$ spinors separated by an increasing energy difference. This is in line with the SO splitting calculated directly for the frontier π-orbital of HX as shown by the data in Table IV. As a consequence of lowering the energy of the valence $p_{1/2}$ spinor, its contribution to σ-bonding is reduced and the bond length increases. Simultaneously, the radial extension of the $p_{3/2}$ spinor increases, thus leading to a further lengthening of the H–X bond with increasing atomic number of X, which has also been found by other authors.[47,66,67]

We note that similar conclusions can be drawn if one starts from the MOs of HX (Figure 2) and considers that SO splitting leads to a mixing between spinors of the same j-value. In the case of HX, the nonbonding HOMS $\pi_{1/2}$ mixes with the antibonding LUMS $\sigma^+_{1/2}$, which leads to bond lengthening. Yet, another possible explanation of the bond length changes in the HX series is obtained by considering that ground and low-lying excited states can interact because of SOC. In the case of HX, this would imply an interaction of the $^1\Sigma^+_{0+}$ ground state and the $^3\Pi_{0+}$ state (possible due to SOC), which has an electron in the antibonding $\sigma^+_{1/2}$ spinor. Hence, this interaction leads to an increase in the HX bond length, which is the stronger, the smaller the excitation energy is. From Cl to At, the excitation energy decreases (because of the smaller H,X electronegativity difference and larger polarizability of X[68]) thus leading to stronger SOC and a stronger lengthening of the bond.[69]

Au–X and Hg–X molecules. For molecules AuX, SOC causes to slight shortening of the AuX bond length where for X = F, the largest decrement is obtained (−0.0073 Å, Table III). This is due to the fact that the $\pi_{1/2}$ HOMS is strongly antibonding whereas the $\sigma^+_{1/2}$ LUMS is weakly bonding (for the frontier orbitals of AuBr, see Figure 2) thus leading to an overall stabilizing effect. Since the LUMS bonding character decreases from F to Br, the bond strengthening decreases in the same direction.

For doublet radicals $HgX(^2\Sigma^+)$ with a fractional occupation of the p-orbitals, a relatively strong variation of the Hg–X bond length ranging from −0.0159 (H) to 0.0149 Å (I) is calculated. In the case of HgBr, HOMO and LUMO are of σ^+ and π symmetry (Figure 2). The dominant antibonding character of the $\sigma^+_{1/2}$ HOMS is lowered by an admixture of the $\pi_{1/2}$ LUMS, which is less antibonding thus leading to a decrease of the bond length. The antibonding character of the LUMS increases with decreasing electronegativity and increasing atomic number of X, which causes a reversal of bond shortening and lengthening due to SOC as found for $HgI(^2\Sigma^+)$ (see Table III).

X–Hg–X molecules. With the exception of X = I, SOC leads to a shortening of the Hg–X bond. The largest shortening (−0.0042 Å, Table III) is found for X = H. Values of −0.0019, −0.0024, −0.0020, and 0.0017 Å are calculated for X = F, Cl, Br, and I, respectively. The frontier spinor interaction is between the $\pi_{g\,1/2}$ spinor forming the HOMS and the $\sigma^+_{g\,1/2}$ forming the LUMS where the former is antibonding and the latter bonding (for the frontier MOs of $HgBr_2$, see Figure 2). Hence, a shortening of the bonds results, which is strongest for X = H. In the HgX_2 molecules with large X, the π_u HOMO−1 interaction with the π_u LUMO+1 (Figure 2) becomes increasingly important (see Table IV), which leads to strong HgX π-antibonding and accordingly to a lengthening of the HgX bond as found for X = I.

HgX_4 molecules. For HgX_4, SOC has a smaller influence on bond lengths than for HgX_2 and HgX. As in the case

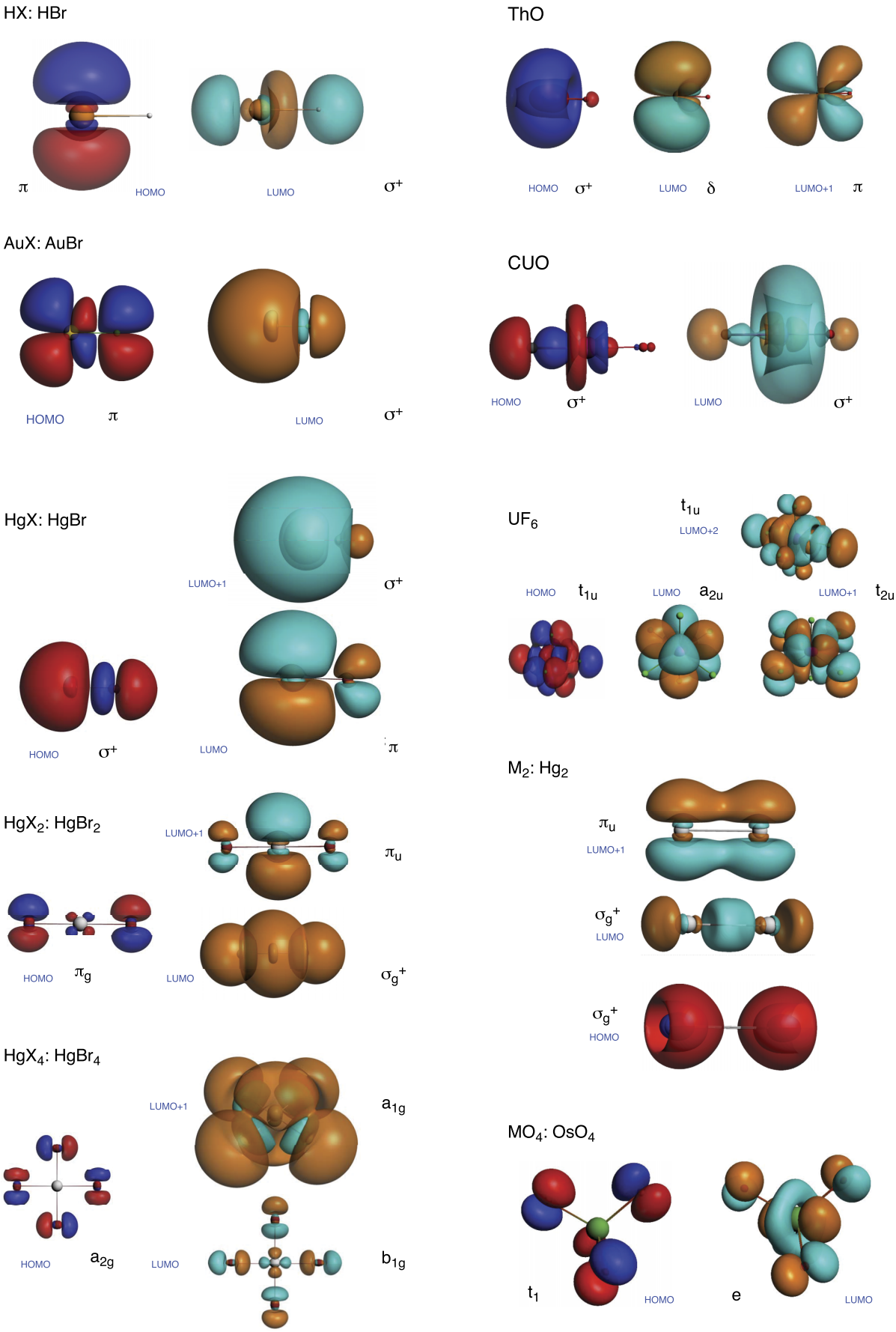

FIG. 2. Perspective drawings of scalar relativistic frontier molecular orbitals of some reference molecules. For molecules HX, AuX, and HgX_n, orbitals for X = Br are shown. In each case, HOMO(−1) and LUMO(+1) as well as their symmetry are given. For the calculated orbital and spinor energies, see Table IV.

TABLE IV. NESC orbital and 2c-NESC spinor energies in hartees. For $HgX(^2\Sigma^+)$, spin-α orbitals are given. For closed-shell linear molecules with $C_{\infty v}$ symmetry, the symmetries and energies of frontier molecular spinors are also given as well as the SO splitting values $E(l+1/2)-E(l-1/2)$.

No.	Molecule	HOMO−1	HOMO	LUMO	LUMO+1	HOMS−1	HOMS	LUMS	LUMS+1	SO splitting
1	HF	σ^+ −0.570	π −0.433	σ^+ 0.016	σ^+ 0.283	1/2−0.434	3/2 −0.433	1/2 0.016	1/2 0.283	0.001 (π)
2	HCl	σ^+ −0.489	π −0.438	σ^+ 0.001	σ^+ 0.121	1/2−0.350	3/2 −0.347	1/2 0.001	1/2 0.121	0.003 (π)
3	HBr	σ^+ −0.460	π −0.321	σ^+ −0.014	σ^+ 0.112	1/2−0.327	3/2 −0.315	1/2 −0.014	1/2 0.112	0.012 (π)
4	HI	σ^+ −0.421	π −0.291	σ^+ −0.028	σ^+ 0.102	1/2−0.302	3/2 −0.279	1/2 −0.028	1/2 0.102	0.023 (π)
5	HAt	σ^+ −0.409	π −0.277	σ^+ −0.045	σ^+ 0.004	1/2−0.307	3/2 −0.246	1/2 −0.047	1/2 0.002	0.061 (π)
6	AuH	δ −0.319	σ^+ −0.273	σ^+ −0.085	π 0.005	5/2 −0.298	1/2 −0.271	1/2 −0.086	1/2 −0.002	0.015 (δ), 0.013 (π)
7	AuF	π −0.320	σ^+ −0.305	σ^+ −0.146	π 0.007	3/2 −0.309	1/2 −0.297	1/2 −0.146	1/2 −0.002	0.017 (π), 0.014 (π)
8	AuCl	σ^+ −0.308	π −0.294	σ^+ −0.138	π 0.005	1/2 −0.292	3/2 −0.288	1/2 −0.139	1/2 −0.003	0.004 (π), 0.015 (π)
9	AuBr	σ^+ −0.305	π −0.281	σ^+ −0.136	π 0.004	1/2 −0.287	3/2 −0.273	1/2 −0.137	1/2 −0.004	0.014 (π), 0.015 (π)
10	Au_2	σ_u^+ −0.278	σ_g^+ −0.262	σ_u^+ −0.123	π_u −0.013					
11	HgH	σ^+ −0.360	σ^+ −0.211	π −0.023	σ^+ 0.071					
12	HgH_2	σ_g^+ −0.364	σ_u^+ −0.298	π_u −0.023	σ_g^+ 0.034					
13	HgH_4	a_{1g} −0.442	e_u −0.320	b_{1g} −0.044	b_{2u} −0.038					
14	HgF	π −0.366	σ^+ −0.281	π −0.026	σ^+ 0.032					
15	HgF_2	σ_g^+ −0.412	π_g −0.377	σ_g^+ −0.083	π_u −0.015					
16	HgF_4	e_g −0.436	b_{2g} −0.434	b_{1g} −0.238	a_{1g} −0.053					
17	HgCl	π −0.317	σ^+ −0.265	π −0.029	σ^+ 0.031					
18	$HgCl_2$	π_u −0.353	π_g −0.327	σ_g^+ −0.082	π_u −0.021					
19	$HgCl_4$	e_g −0.353	a_{2g} −0.330	b_{1g} −0.229	a_{1g} −0.061					
20	HgBr	π −0.299	σ^+ −0.259	π −0.029	σ^+ 0.024					
21	$HgBr_2$	π_u −0.328	π_g −0.307	σ_g^+ −0.089	π_u −0.023					
22	$HgBr_4$	e_u −0.321	a_{2g} −0.298	b_{1g} −0.221	a_{1g} −0.076					
23	HgI	π −0.278	σ^+ −0.250	π −0.029	σ^+ 0.023					
24	HgI_2	π_u −0.300	π_g −0.283	σ_g^+ −0.093	π_u −0.027					
25	HgI_4	e_u −0.287	a_{2g} −0.265	b_{1g} −0.207	a_{1g} −0.091					
26	Hg_2	σ_g^+ −0.299	σ_u^+ −0.258	σ_g^+ −0.031	π_u −0.025					
27	ThO	σ^+ −0.337	σ^+ −0.174	δ −0.077	π −0.062	1/2 −0.337	1/2 −0.175	3/2 −0.085	5/2 −0.072	0.013 (δ), 0.014 (π)
28	CUO	π −0.223	σ^+ −0.193	σ^+ −0.082	ϕ −0.070	3/2 −0.224	1/2 −0.194	5/2 −0.090	1/2 −0.079	0.006 (π), 0.029 (ϕ)
29	UF_6	t_{1g} −0.468	t_{1u} −0.446	a_{2u} −0.220	t_{2u} −0.199					
30	OsO_4	t_2 −0.417	t_1 −0.388	e −0.151	t_2 −0.065					
31	HsO_4	t_2 −0.408	t_1 −0.388	e −0.129	t_2 −0.051					
32	Cn_2	π_g −0.349	σ_u^+ −0.341	σ_g^+ −0.028	π_u −0.026					

of the HgX and the HgX_2 molecules, SOC leads to a maximum bond shortening for X = H followed by X = Cl, which is then reverted so that the Hg–X bond lengths increase for X = Br and I by ΔR_{soc} = 0.0012 and 0.0156 Å, respectively (Table III). Again, this is a result of the fact that the frontier spinors are antibonding where however for X = F, the HOMS is more antibonding than the LUMS and for X = I, the situation is reverted (for the frontier MOs, see Figure 2) as a result of the change in the electronegativity differences from $\chi(Hg) - \chi(F)$ to $\chi(Hg) - \chi(I)$.[68]

Tetroxides OsO_4 and HsO_4, thorium oxide, ThO, and uranium carbide oxide, CUO. The slightly antibonding LUMO t_1 and the nonbonding e HOMO of MO_4 (M = Os, Hs, Figure 2) can mix in the $f_{3/2}$ irreducible representation via SOC, which leads to a slight MO bond length increase. For M = Os and Hs, 0.0002 and 0.0040 Å are calculated again confirming that SOC effects increase with increasing atomic number (Table III). In the case of ThO, LUMO and LUMO+1 (Figure 2) are very close in energy (see Table IV). The LUMO is a non-bonding orbital, and the LUMO+1 is a weakly bonding orbital. The $\pi_{1/2}$ LUMS+1 and the $\sigma_{1/2}^+$ HOMS can mix due to SOC thus causing a decrease of the Th–O bond length.

For the uranium carbide oxide, which has a shorter UC bond (1.725) and a somewhat longer UO bond (1.759 Å, Table III), the LUMO is a bonding orbital (weakly bonding for UC and strongly bonding for UO), whereas the HOMO is antibonding (strongly for UC and weakly for UO, see Figure 2). After SOC being taken into account, the σ^+ HOMO and σ^+ LUMO mix and lead to two new 1/2 spinors, which causes both bond lengths to decrease with the UO bond being more shortened (−0.0200 Å).

Uraniumhexafluoride, UF_6. LUMO, LUMO+1, and LUMO +2 are very close in energy (see Table IV). The HOMO is U–F antibonding, the LUMO non-bonding, the LUMO+1 antibonding, and the LUMO+2 U–F bonding (see Figure 2). When SOC is taken into account, HOMO, LUMO+1, and LUMO+2 mix and lead to new $e_{1/2u}$, $e_{5/2u}$, and $f_{3/2u}$ spinors with the result that the U–F bond lengths slightly decrease (ΔR_{soc} = −0.0038 Å, Table III).

Diatomic molecule Au_2 and van der Waals complexes Hg_2 and Cn_2. For the closed-shell covalently bonded Au_2 molecule, a much smaller SOC reduction of its M,M distance (−0.0047 Å) is found than for the van der Waals molecules Hg_2 and Cn_2 (−0.0476 and −0.4453 Å, Table III). The

HOMO of the van der Waals complexes M_2 (M = Hg, Cn) is a weakly bonding orbital whereas LUMO and LUMO+1 are strongly bonding orbitals (see Figure 2). A mixing of the σ_g^+ HOMO and the σ_g^+ LUMO due to SOC leads to two new $1/2_g$ spinors, which cause a substantial bond strengthening. An additional bond strengthening effect results from the mixing of the π_u LUMO+1 and the σ_u^+ HOMO−1 (not shown in Figure 2) in form of $1/2_u$ spinors. The bond length reduction of −0.0476 (Hg_2) and −0.4453 Å (Cn_2, Table III) is 3.5 and 2.2 times larger than the corresponding scalar relativistic reduction (−0.0135 and −0.2016 Å). This is a result of a relatively flat potential energy surface in the vicinity of the location of the van der Waals complexes where small changes in the frontier orbitals lead to large ΔR_{soc} changes. The Cn,Cn interaction distance is calculated to be 3.255 Å in agreement with other predictions made in this work with the PBE0 functional (X2C/AMFI: 3.261 and 4c-Dirac Kohn-Sham: 3.256 Å). Similar interaction distances have been obtained by Hangele and Dolg who compared 4c- and 2c-DFT descriptions of Cn_2 with 2c-CC descriptions.[70]

V. CONCLUSIONS

The analytical gradient of the 2c-NESC(mSNSO) method has been developed and implemented into the 2c-NESC program. The accuracy of the analytical gradient was confirmed by a comparison with numerical gradients. Test calculations reveal that the mSNSO(W) screened-nuclear-spin-orbit approach does not lead to any significant deterioration of calculated SO splittings relative to those obtained with the mSNSO(H) approach (scaling of **H**-matrix elements). 2c-NESC(mSNSO) geometry optimizations using the analytical gradient were carried out for 32 molecules. Scalar relativistic changes lead to a bond length shortening when bonding is dominated by *s*- and/or *p*-orbital contributions whereas a dominance of *d*- or *f*-orbitals leads to bond lengthening as shown in this work for CUO. SOC effects can also lead to either bond lengthening or shortening. It is shown that this is a result of frontier orbital mixing where due to SOC, orbitals of the same quantum number *j* can mix. Inspection of orbital energy differences, SO splittings, and the character of the frontier orbitals (bonding, non-bonding, or antibonding) makes it possible to qualitatively explain the calculated ΔR_{soc} values. For molecules containing strongly relativistic elements with atomic numbers 80 or larger, a calculation of ΔR_{soc} is necessary to make reliable predictions for their equilibrium geometries.

ACKNOWLEDGMENTS

This work was financially supported by the National Science Foundation, Grant No. CHE 1152357. We thank SMU for providing computational resources. Also, we acknowledge the suggestion of an unknown referee to simplify Eq. (19).

[1]W. Zou, M. Filatov, and D. Cremer, Theor. Chem. Acc. **130**, 633 (2011).
[2]W. Zou, M. Filatov, and D. Cremer, J. Chem. Phys. **134**, 244117 (2011).
[3]W. Zou, M. Filatov, and D. Cremer, J. Chem. Phys. **137**, 084108 (2012).
[4]K. G. Dyall, J. Chem. Phys. **106**, 9618 (1997).
[5]P. A. M. Dirac, Proc. R. Soc. (London) **A117**, 610 (1928).
[6]M. Filatov, W. Zou, and D. Cremer, J. Phys. Chem. A **116**, 3481 (2012).
[7]M. Filatov, W. Zou, and D. Cremer, J. Chem. Theor. Comput. **8**, 875 (2012).
[8]M. Filatov, W. Zou, and D. Cremer, J. Chem. Phys. **137**, 054113 (2012).
[9]W. Zou, M. Filatov, and D. Cremer, J. Chem. Theory Comput. **8**, 2617 (2012).
[10]W. Zou, M. Filatov, D. Atwood, and D. Cremer, Inorg. Chem. **52**, 2497 (2013).
[11]M. Filatov, W. Zou, and D. Cremer, J. Chem. Phys. **137**, 131102 (2012).
[12]E. Kraka, W. Zou, M. Freindorf, and D. Cremer, J. Chem. Theory Comput. **8**, 4931 (2012).
[13]K. G. Dyall and K. Fægri, *Introduction to Relativistic Quantum Chemistry* (Oxford University Press, Oxford, 2007).
[14]T. R. Furlani and H. F. King, J. Chem. Phys. **82**, 5577 (1985).
[15]D. G. Fedorov, S. Koseki, M. W. Schmidt, and M. S. Gordon, Int. Rev. Phys. Chem. **22**, 551 (2003).
[16]C. M. Marian, WIREs Comput. Mol. Sci. **2**, 187 (2012).
[17]W. Liu, Mol. Phys. **108**, 1679 (2010).
[18]T. Saue, ChemPhysChem **12**, 3077 (2011).
[19]D. Peng and M. Reiher, Theor. Chem. Acc. **131**, 1081 (2012).
[20]T. Fleig, Chem. Phys. **395**, 2 (2012).
[21]M. Reiher and A. Wolf, *Relativistic Quantum Chemistry, The Fundamental Theory of Molecular Science*, 2nd ed. (Wiley-VCH, Weinheim, 2015).
[22]M. Filatov, W. Zou, and D. Cremer, J. Chem. Phys. **139**, 014106:1 (2013).
[23]D. G. Fedorov and M. S. Gordon, J. Chem. Phys. **112**, 5611 (2000).
[24]O. Vahtras, M. Engström, and B. Schimmelpfennig, Chem. Phys. Lett. **351**, 424 (2002).
[25]J. Tatchen, M. Kleinschmidt, and C. M. Marian, J. Chem. Phys. **130**, 154106 (2009).
[26]J. C. Boettger, Phys. Rev. B **62**, 7809 (2000).
[27]M. Douglas and N. M. Kroll, Ann. Phys. **82**, 89 (1974).
[28]B. A. Hess, Phys. Rev. A **32**, 756 (1985).
[29]B. A. Hess, Phys. Rev. A **33**, 3742 (1986).
[30]S. Majumder, A. V. Matveev, and N. Rösch, Chem. Phys. Lett. **382**, 186 (2003).
[31]J. E. Peralta and G. E. Scuseria, J. Chem. Phys. **120**, 5875 (2004).
[32]C. van Wüllen and C. Michauk, J. Chem. Phys. **123**, 204113 (2005).
[33]J. Chalupsky and T. Yanai, J. Chem. Phys. **139**, 204106 (2013).
[34]B. Schimmelpfennig, *AMFI: Atomic Mean Field Integral Program* (University of Stockholm, Stockholm, Sweden, 1996).
[35]B. A. Hess, C. M. Marian, U. Wahlgren, and O. Gropen, Chem. Phys. Lett. **251**, 365 (1996).
[36]A. Berning, M. Schweizer, H.-J. Werner, P. J. Knowles, and P. Palmieri, Mol. Phys. **98**, 1823 (2000).
[37]S. Coriani, T. Helgaker, P. Jørgensen, and W. Klopper, J. Chem. Phys. **121**, 6591 (2004).
[38]R. Seeger and J. A. Pople, J. Chem. Phys. **66**, 3045 (1977).
[39]S. Hammes-Schiffer and H. C. Andersen, J. Chem. Phys. **99**, 1901 (1993).
[40]M. Iliaš and T. Saue, J. Chem. Phys. **126**, 064102 (2007).
[41]W. Liu and D. Peng, J. Chem. Phys. **125**, 044102 (2006).
[42]W. Liu and D. Peng, J. Chem. Phys. **125**, 149901 (2006).
[43]W. Liu, Phys. Rep. **537**, 59 (2014).
[44]E. van Lenthe, A. Ehlers, and E.-J. Baerends, J. Chem. Phys. **110**, 8943 (1999).
[45]F. Wang and J. Gauss, J. Chem. Phys. **129**, 174110 (2008).
[46]Z. Zhang, Theor. Chem. Acc. **133**, 1588 (2014).
[47]C. S. Nash and B. E. Bursten, J. Phys. Chem. A **103**, 632 (1999).
[48]F. Aquino, N. Govind, and J. Autschbach, J. Chem. Theory Comput. **6**, 2669 (2010).
[49]J. Autschbach, D. Peng, and M. Reiher, J. Chem. Theory Comput. **8**, 4239 (2012).
[50]S. Varga, A. Rosén, W.-D. Sepp, and B. Fricke, Phys. Rev. A **63**, 022510 (2001).
[51]F. Wang and L. Li, J. Comput. Chem. **23**, 920 (2002).
[52]T. Shiozaki, J. Chem. Theory Comput. **9**, 4300 (2013).
[53]DIRAC, a relativistic *ab initio* electronic structure program, Release DIRAC12 (2012), written by H. J. Aa. Jensen, R. Bast, T. Saue, and L. Visscher, with contributions from V. Bakken, K. G. Dyall, S. Dubillard, U. Ekström, E. Eliav, T. Enevoldsen, T. Fleig, O. Fossgaard, A. S. P. Gomes, T. Helgaker, J. K. Lærdahl, Y. S. Lee, J. Henriksson, M. Iliaš, Ch. R. Jacob, S. Knecht, S. Komorovský, O. Kullie, C. V. Larsen, H. S. Nataraj, P. Norman, G. Olejniczak, J. Olsen, Y. C. Park, J. K. Pedersen, M. Pernpointner, K. Ruud, P. Sałek, B. Schimmelpfennig, J. Sikkema, A. J. Thorvaldsen, J. Thyssen, J. van Stralen, S. Villaume, O. Visser, T. Winther, and S. Yamamoto (see http://www.diracprogram.org).
[54]V. Kellö and A. J. Sadlej, J. Mol. Struct. (THEOCHEM) **547**, 35 (2001).

[55]K. G. Dyall, J. Comput. Chem. **23**, 786 (2002).
[56]W. Liu and D. Peng, J. Chem. Phys. **131**, 031104 (2009).
[57]COLOGNE, a quantum chemical electronic structure program, Release COLOGNE15 (2015), written by E. Kraka, M. Filatov, W. Zou, J. Gräfenstein, D. Izotov, J. Gauss, Y. He, A. Wu, V. Polo, L. Olsson, Z. Konkoli, Z. He, and D. Cremer (Southern Methodist University, Dallas, TX).
[58]L. Visscher and K. G. Dyall, At. Data Nucl. Data Tables **67**, 207 (1997).
[59]G. Gabrielse, D. Hanneke, T. Kinoshita, M. Nio, and B. Odom, Phys. Rev. Lett. **97**, 030802 (2006).
[60]A. Wolf, M. Reiher, and B. A. Hess, J. Chem. Phys. **117**, 9215 (2002).
[61]G. L. Malli, A. B. F. D. Silva, and Y. Ishikawa, J. Chem. Phys. **101**, 6829 (1994).
[62]J. P. Perdew, K. Burke, and M. Ernzerhof, Phys. Rev. Lett. **77**, 3865 (1996).
[63]C. Adamo and V. Barone, J. Chem. Phys. **110**, 6158 (1999).
[64]F. Weigend and R. Ahlrichs, Phys. Chem. Chem. Phys. **7**, 3297 (2005).
[65]W. A. de Jong, L. Visscher, and W. C. Nieuwpoort, J. Mol. Struct. (THEOCHEM) **458**, 41 (1998).
[66]L. Visscher, J. Styszyński, and W. C. Nieuwpoort, J. Chem. Phys. **105**, 1987 (1996).
[67]T. Saue, K. Faegri, and O. Groppen, Chem. Phys. Lett. **263**, 360 (1996).
[68]D. R. Lide, *CRC Handbook of Chemistry and Physics*, 90th ed. (CRC, Boca Raton, FL, 2009-2010).
[69]K. P. Huber and G. Herzberg, *Molecular Spectra and Molecular Structure IV. Constants of Diatomic Molecules* (Van Nostrand Reinhold, New York, 1979).
[70]T. Hangele and M. Dolg, Chem. Phys. Lett. **616-617**, 222 (2014).
[71]D. A. Pantazis, X.-Y. Chen, C. R. Landis, and F. Neese, J. Chem. Theory Comput. **4**, 908 (2008).
[72]D. A. Pantazis and F. Neese, J. Chem. Theory Comput. **7**, 677 (2011).
[73]H. Tatewaki and T. Koga, Chem. Phys. Lett. **328**, 473 (2000).
[74]Data base of Segmented Gaussian Basis Sets, Quantum Chemistry Group, Sapporo, Japan (2014), http://setani.sci.hokudai.ac.jp/sapporo/Welcome.do.
[75]K. G. Dyall, Theor. Chem. Acc. **129**, 603 (2011).
[76]T. Okabayashi, Y. Nakaoka, E. Yamazaki, and M. Tanimoto, Chem. Phys. Lett. **366**, 406 (2002).
[77]L. M. Reynard, C. J. Evans, and M. C. L. Gerry, J. Mol. Spectrosc. **205**, 344 (2001).
[78]G. A. Bishea and M. D. Morse, J. Chem. Phys. **95**, 5646 (1991).
[79]J. Dufayard, B. Majournat, and O. Nedelec, Chem. Phys. **128**, 537 (1988).
[80]A. Shayesteh, S. Yu, and P. F. Bernath, J. Phys. Chem. A **109**, 10280 (2005).
[81]A. K. Rai, S. B. Rai, and D. K. Rai, J. Phys. B: At. Mol. Phys. **15**, 3239 (1982).
[82]J. Tellinghuisen and J. G. Ashmore, Appl. Phys. Lett. **40**, 867 (1982).
[83]J. Tellinghuisen, P. C. Tellinghuisen, S. A. Davies, P. Berwanger, and K. S. Viswanathan, Appl. Phys. Lett. **41**, 789 (1982).
[84]V. S. Zuev, J. G. Eden, and H. C. Tran, Opt. Spectrosc. **90**, 516 (2001).
[85]V. Goncharov and M. C. Heaven, J. Chem. Phys. **124**, 064312 (2006).
[86]M. Kimura, V. Schomaker, D. W. Smith, and B. Weinstock, J. Chem. Phys. **48**, 4001 (1968).
[87]B. Krebs and K.-D. Hasse, Acta Crystallogr., Sect. B: Struct. Crystallogr. Cryst. Chem. **32**, 1334 (1976).